




Comparing polarized Raman spectroscopy and birefringence as probes of molecular scale alignment in 3D printed thermoplastics

Nora M. Hassan, Hopkins Extreme Materials Institute, Johns Hopkins University, Baltimore, MD, USA; Material Measurement Laboratory, National Institute of Standards and Technology, Gaithersburg, MD, USA; Physical Measurement Laboratory, National Institute of Standards and Technology, Gaithersburg, MD, USA

Kalman B. Migler, Material Measurement Laboratory, National Institute of Standards and Technology, Gaithersburg, MD, USA

Angela R. Hight Walker, Physical Measurement Laboratory, National Institute of Standards and Technology, Gaithersburg, MD, USA

Anthony P. Kotula, Jonathan E. Seppala , Material Measurement Laboratory, National Institute of Standards and Technology, Gaithersburg, MD, USA

Address all correspondence to Anthony P. Kotula at anthony.kotula@nist.gov and Jonathan E. Seppala at jonathan.seppala@nist.gov

(Received 22 December 2020; accepted 23 February 2021)

Abstract

Polymer chain orientation is crucial to understanding the polymer dynamics at interfaces formed during thermoplastic material extrusion additive manufacturing. The flow field and rapid cooling produced during material extrusion can result in chains which are oriented and stretched, which has implications for interdiffusion and crystallization. Polarized Raman spectroscopy offers a non-destructive and surface sensitive method to quantify chain orientation. To study orientation and alignment of chains in 3D printed polycarbonate filaments, we used a combination of polarized Raman spectroscopy and birefringence (Δn) measurements. By changing the orientation of the sample with respect to polarization of incident radiation, we probe changes in the ratio between orientation-dependent vibration modes and orientation-independent modes. We used principal component analysis (PCA) and partial least squares (PLS) regression to develop correlations for birefringence and Raman measurements in samples that were pulled at different draw ratios (DRs). PCA was used to differentiate between orientation-dependent and orientation-independent modes, while PLS regression was used to calculate birefringence from Raman measurements of 3D printed samples. Birefringence measurements were compared to the polycarbonate intrinsic birefringence of 0.2, to estimate the degree of orientation. We find that measured values of birefringence underestimate orientation compared to Raman measurements.

Introduction

Thermoplastic material extrusion (MatEx)¹ additive manufacturing (AM) is growing exponentially due to its wide application space, short lead time, low expense, and the ability to manufacture complex 3D parts that cannot be manufactured using traditional manufacturing methods such as machining.^[1] Thermoplastic MatEx is a particular implementation of AM where thermoplastic filament is extruded layer-by-layer to make a 3D printed part. The filament is fed into a heated extruder where it is melted and extruded as a molten filament with a specific diameter through a nozzle. Through the motion of the extruder head and the build bed in the x , y and z directions, the extrudate is printed layer-by-layer and a 3D object is constructed, see Fig. 1(a). However, it is very difficult to implement quality assurance and control in AM, such as carefully testing to ensure consistent part quality that is checked against certain criteria, including dimensional accuracy, porosity, or mechanical properties such as tensile strength. That difficulty is due to strong dependence of electrical, optical, thermal, and mechanical properties^[2] on the various printing parameters such as extruder head temperature, the speed of printing, layer

thickness, and printing direction. Therefore, for AM to be a dependable and mainstream process in manufacturing, a thorough understanding of the effect of these parameters on the dynamic and microscopic behavior of the molecular structure is crucial.

It has been shown that printing temperature and printing speed are the most important parameters^[2-5] that affect the mechanical properties of 3D printed objects, and the variation in these parameters are the main culprit to the inconsistency in part quality. Therefore, theoretical and experimental efforts have been studied to understand the effects of these parameters on the mechanical properties. Experimental results have shown that weld areas between filaments experience mechanical failure more often than at the bulk.^[2,6] Various theoretical models have predicted that failure tends to take place near the weld area due to the poor inter-molecular entanglement at the weld-line interface which is in part attributed to alignment of chains of the polymer. A 3D structure is built by extruding polymer melt from the nozzle at temperatures greater than the glass transition temperature $T > T_g$ where the molten extrudate also heats the sublayer above T_g , see Fig. 1(a). It is believed that

Official contribution of the National Institute of Standards and Technology; not subject to copyright in the United States.

¹ Material extrusion is the ASTM definition for this process; however, it is also known as fused deposition modeling (FDM)[®] or fused filament fabrication (FFF).

the polymer chain is oriented and extended under shear flow as the polymer is extruded from the nozzle and that this shear during extrusion and cooling leads to varying chain alignment within the extrudate. Models predicted the orientation profile of the chain as they are sheared through the nozzle; across the diameter of the extrudate, the surface has highest chain orientation, and the center has the lowest orientation.^[7] Additionally, as they cool, some of the chains in the sublayer relax and lose some of their orientation. A weld is formed with prior layers by diffusion of chains across the interface until T drops below T_g . Rapid cooling during and after deposition preserves print shape but freezes-in chain alignment and limits interdiffusion. On the other hand, a recent work has proposed that the weld strength reduction is due not to a reduction in inter-layer entanglement, but rather to a modification of the configuration of the entangled polymer network in the glassy state.^[8] In all such theoretical considerations, the alignment of the polymer in the weld region is a crucial factor, both in terms of the kinetics of the printing process and the final strength.

Different techniques such as nuclear magnetic resonance,^[9] X-ray scattering measurements,^[10–12] birefringence,^[13] infrared^[12,14–17] and Raman spectroscopy^[12,15,18–26] have been used to determine chain orientation in polymers especially in polymers such as polystyrene, polyethylene terephthalate, and polylactic acid. Most measurements of chain orientation were studied in the context of the injection molding process, while less is known about chain orientation in AM processes.^[27] Because the chain orientation is among the important parameters in determining the strength in the weld area, it is crucial to estimate the orientation accurately. Birefringence is a promising method due to its high sensitivity to alignment, and has been employed by Costanzo et al.^[8] to measure alignment during AM. However, transmission/bulk techniques, such as birefringence, will mostly underestimate the orientation because it provides an average of chain orientation across the cross-section of the extrudate. In contrast, confocal Raman is surface sensitive and probes few microns from the surface, and using polarized Raman excitation and collection, chain orientation on the monomer level can be probed. It provides better depth resolution ($\approx 5 \mu\text{m}$), provides richer information that can be extracted, such as second- and fourth-order moments of the segment orientation distribution that can be correlated with optical birefringence^[9,19] and is a non-destructive method that needs no sample preparation. The methods mentioned earlier probe chain orientation on the monomer level, i.e., they probe the distribution of angles that the bonds within monomers make with a specific axis, see Fig. 1(b). However, much of the theoretical work^[28] was done to predict chain orientation in the chain end-to-end scale where the distance between the chain ends is what matters in determining chain orientation and weld area strength. It is quite possible to have orientation at the end-to-end scale with low orientation in the monomer scale.^[29,30] In this article we present an analysis of polarized Raman spectra and birefringence of amorphous polycarbonate (PC) samples to generate an empirical relation between the two methods to

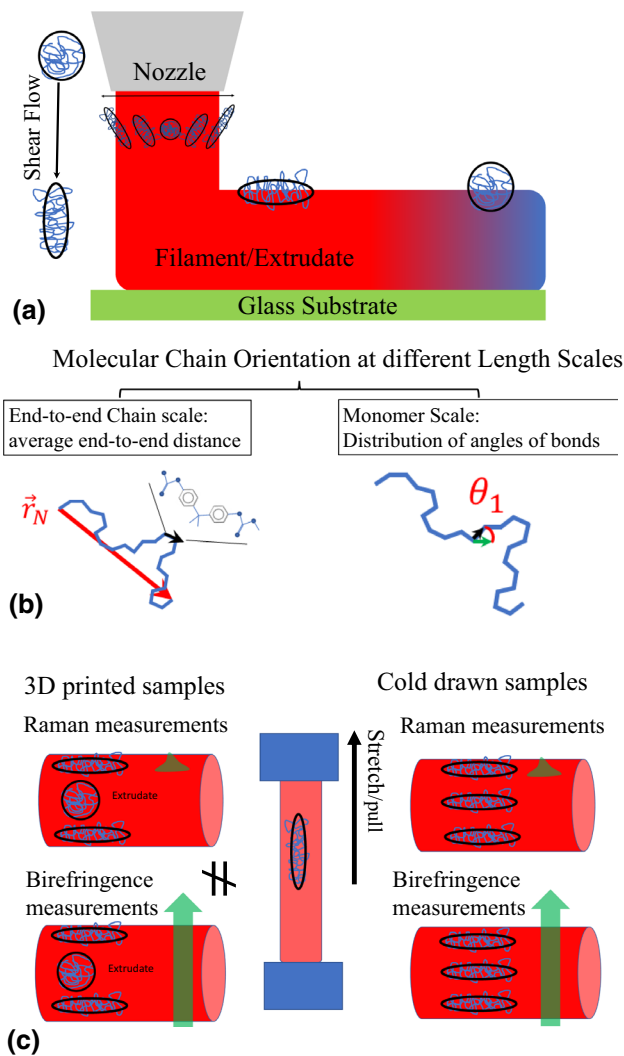


Figure 1. (a) A polycarbonate sample/extrudate (red) is extruded from a nozzle (gray) at a certain printing temperature as the nozzle moves to the left. As the filament is extruded, the surface in contact with the nozzle wall experiences more shear forces and thus, the non-oriented chain (blue) within the filament extends to achieve better orientation (chains not shown to scale). Across the diameter of the extrudate, the surface has highest chain orientation and the center lowest orientation. (b) The degree of chain orientation can be evaluated based on two length scales: the end-to-end length scale and monomer length scale. In the end-to-end length scale, the chain orientation is evaluated based on the average distance between the two ends of the chain, while on the monomer scale the chain orientation is evaluated based on the distribution of bond angles. The latter is measured by Raman spectroscopy and birefringence, the former, however, is not probed by either methods. (c) On the left, Raman spectroscopy measurements, a surface method, and birefringence measurements are not equivalent because in 3D printed samples, there is more orientation on the surface. To accurately relate birefringence and Raman scattering measurements, a training set was used where the samples were briefly annealed (5 min) and then stretched/pulled to different DRs to achieve different degrees of molecular chain orientation (right panel). In the training set, the degree of orientation of chains is similar across the diameter of the filament and so a surface method such as Raman scattering and a transmission method such as birefringence can be related reliably.

predict a value of birefringence that better describes chain orientation due to shear effects in AM. It is worth mentioning that the current work presented in this article is concerned with chain orientation at surface of the filaments due to shearing forces introduced by the nozzle. The work recently published by Costanzo et al.^[8] probes the chain orientation in the weld area using birefringence measurements. Their birefringence measurements, albeit done without any index matching fluid and thus could misrepresent birefringence values, measures the alignment at the weld area due to the convolution of many factors such as the shearing forces of nozzle, the bending of the filament as it is being printed and other factors.

To accurately relate a surface method such as Raman spectroscopy to a bulk measurement method that depends on transmission such as birefringence, it should be emphasized that chain orientation must be mostly uniform throughout the cross-section of the filaments. This is achieved by stretching the samples through cold drawing of the PC filaments, after a short anneal, to different DRs. This is illustrated in Fig. 1(c); in AM where most orientation is on the surface of the sample, a surface method will more accurately predict orientation, while a transmission method will most likely underestimate the orientation on the surface, most relevant and important in weld area mechanics, by averaging over the cross-section of the sample. Thus, it could be less accurate to relate these two methods directly in injection molded or 3D printed samples. A better method is to use a training set of samples that have more or less the same molecular orientation throughout the cross-section. Thus, the probed volumes in both methods have similar orientation profile and a direct correspondence between a transmission method and a surface methods can be made.

Experimental

Sample preparation

Polycarbonate (PC) was used as a model amorphous thermoplastic. PC pellets were purchased from Scientific Polymer Products² (Ontario, NY) and used as received. PC spools (2.85 mm nominal diameter) were purchased from AirWolf3D (Las Vegas, NV). Sections of PC spools were dried overnight in a vacuum oven at 60–70 °C before use in the 3D printer. Printed and freely extruded PC samples were prepared on an Axiom Dual Drive Direct material extrusion 3D printer (AirWolf3D, Las Vegas, NV). Freely extruded samples were prepared by extruding filament, in air, at an extrusion temperature of 290 °C and linear feed rate of 10 mm s⁻¹. Samples that were extruded freely in air were approximately 600 μm to 800 μm in diameter. These samples were drawn at 1 mm s⁻¹ and 150 °C

to different DRs using the tensile stage of a force convection oven, equipped with a Dynamic Mechanical Analyzer (DMA)/solid analyzer RSA3 (TA Instruments, New Castle, DE). Prior to drawing, the samples were annealed at 150 °C for several minutes to relax any shear effects from extrusion. After drawing, the samples were quenched by quickly opening the oven to ambient conditions. Draw ratios (defined as $(l_2 - l_1)/l_1$, where l_1 is the initial length of the filament between the two clamps of the DMA and l_2 is the final length after drawing the filament) ranged from 0.04 to 4. Drawn samples were cut in half - one half was used in Raman spectroscopy measurements and the other half was used in birefringence measurements. The measurements were performed at least 0.5 mm from the cut and 5 mm from the clamped region of the sample to avoid regions of non-uniform deformation caused by the clamps during drawing. A second set of printed samples were extruded at nominal temperatures of 220 °C, 240 °C, 260 °C, and 290 °C and a linear feed rate of 10 mm s⁻¹ and were also measured using Raman spectroscopy and birefringence without additional processing.

Raman spectroscopy measurements

Raman spectra were collected at room temperature on a Renishaw Invia microscope using a 514 nm laser, see Fig. 2(a), (b) for an illustration of the setup. Measurements were performed with a 50x objective with numerical aperture $NA = 0.7$. A high confocal setting with a slit width of 25 μm was used in the measurements. Data was collected using either a 1800 lines mm⁻¹ ruled grating and a 12.7 mm charged coupled device (CCD) detector or a 1200 lines mm⁻¹ ruled grating and a 25.4 mm CCD. An approximately 1 μm laser spot delivered approximately 3 mW of polarized light to the sample. Polarized Raman spectra are denoted by the Porto nomenclature,^[31] $W(XY)Z$, where W and Z represent the propagation directions of the incident and scattered light, X and Y represent the direction of polarization of the incident and scattered light. All experiments were carried out in the 180° back scattering geometry, i.e., the path of the propagation of the incident and scattered light is the same but their directions are opposite. Parallel $Z(XX)\bar{Z}$ and cross-polarization $Z(XY)\bar{Z}$ were measured, see Fig. 3.

In all measurements, no change to the optics took place, rather the filaments were rotated with respect to the polarization direction of the incident laser at angles 0°, 45° and 90°. Assuming the chain orientation is along the extrusion direction, the angle is zero when the incident polarization is parallel to the axis of extrudate/flow direction. All measurements were collected in the parallel polarization $Z(XX)\bar{Z}$ by fixing the analyzer and a half wave plate.

Birefringence measurements

Transmission birefringence measurements, see Fig. 2(c) for setup, were collected for every pulled sample. Samples were immersed in a cinnamon bark oil, Sigma-Aldrich, which has an index of refraction 1.573 to 1.591 at 20 °C to match the index

² Certain commercial equipment, instruments, or materials are identified in this paper to specify the experimental procedure adequately. Such identification is not intended to imply recommendation or endorsement by the National Institute of Standards and Technology, nor is it intended to imply that the materials or equipment identified are necessarily the best available for the purpose.

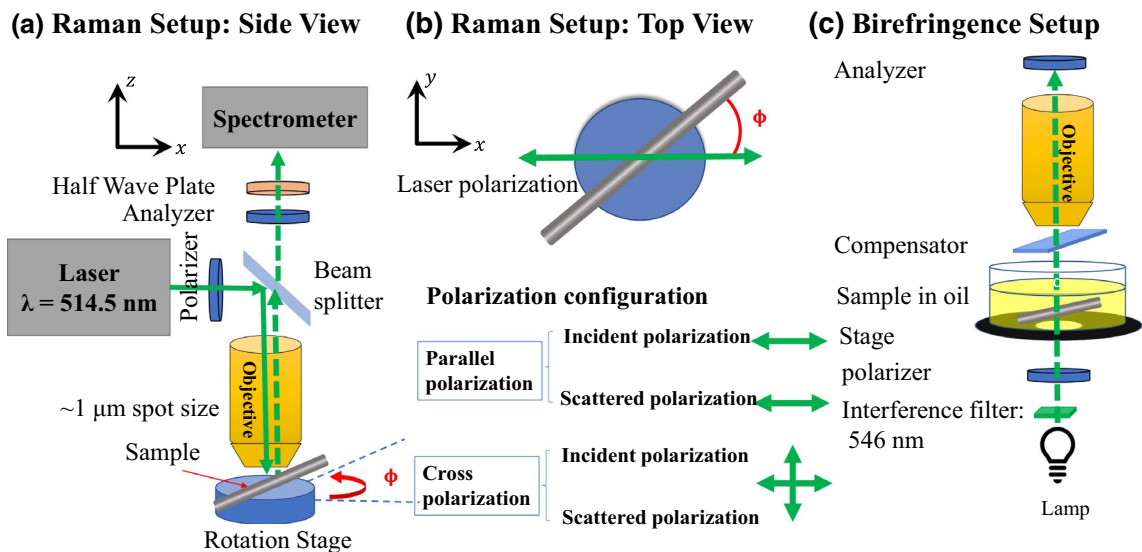


Figure 2. (a) Side view of the Raman setup. 514.5 nm laser and 50 \times objectives were used. The sample is placed on a rotating stage such that the filament is at a certain angle ϕ with respect to the polarization of the laser. ϕ is the angle between the incident laser polarization and filament axis. The scattered Raman goes back through the objective, then through a polarizer and half wave plate before it is dispersed in the spectrometer. (b) Top view of the Raman setup shows the angle between the filament axis and polarization of incident laser. Bottom part shows the different orientation configuration to probe the symmetry of the molecular vibrational modes. (c) Setup of birefringence measurements performed in the transmission mode.

of refraction of the polymer. In the absence of index matching fluid, the curvature of the filaments caused birefringence. As curvature is known to vary with printing conditions, the measured birefringence due to alignment and that due to curvature would be difficult to separate out. We note that Costanzo et al.^[8] does not indicate the use of an index matching fluid. Samples with small birefringence, i.e., retardation of less than one wavelength, were measured using the de Sénarmont compensator. For those with larger birefringence values, i.e., with a retardation of more than one wavelength, a Berek compensator was used. Measurements were collected using an Olympus microscope with a 5 \times objective. Linearly polarized light from the lamp underneath the stage passes through the sample in oil. The sample converts the linearly polarized light into an elliptically polarized light that goes through the compensator and a value of retardation is measured. Diameters of samples were measured by taking images of the filament in oil under the microscope and comparing these to the image of a standard with resolution of 10 μm per marking. By dividing the retardation by the diameter of the sample, a value of birefringence is determined.

Results and discussion

Vibrational modes of pure PC pellets with nominal molecular mass of 45,000 g mol^{-1} are shown in Fig. 3. Due to the presence of additives in commercial PC spools, the spectrum of extruded samples was compared to the modes of pure PC. No Raman modes due to additives could be detected in the spectra of 3D printed samples and all modes could be

attributed to PC vibrations. Figure 3 details PC vibrational spectra in parallel and cross-polarization and the assigned molecular vibrations. Table I shows a list of the vibrational modes of PC.^[32] From comparison of parallel and cross-polarization it is clear that all modes decrease significantly in cross-polarization except those at 635 cm^{-1} and 1600 cm^{-1} that correspond to the phenyl ring stretch where they decrease by < 50%. The C–H stretching mode at 2975 cm^{-1} also shows less decrease in intensity than other modes. Cross and parallel polarization are a manifestation of the molecule symmetry and thus used to study the molecular orientation. The polarization of the incident and scattered radiation are fixed and only the orientation of the sample was varied. Of special interest are modes: 640 cm^{-1} , 709 cm^{-1} , 890 cm^{-1} , 1112 cm^{-1} , 1180 cm^{-1} , 1235 cm^{-1} , and 1602 cm^{-1} corresponding to the phenyl ring, the C–H out-of-plane bending, the O–C(O)–C stretch, the C–O–C stretch and the phenyl ring stretch respectively.

Every sample was annealed for 5 min to 10 min in the solid analyzer at 150 $^{\circ}\text{C}$ before it was pulled to a specific DR. Then birefringence and Raman spectroscopy measurements were collected for each sample. A clear relation between the Raman spectra and measured birefringence can be established because chain orientation is uniform throughout the cross-section of the sample; and so transmission and surface techniques should agree on the extent of orientation. To measure molecular orientation using Raman spectroscopy, spectra of the sample is measured when the sample/filament axis is fixed at angles 0 $^{\circ}$ and 90 $^{\circ}$ with respect to the direction of polarization. Because raw Raman intensity is complex and depends on a variety of

Table I. List of Polycarbonate modes from references.^[32]

Frequency (cm ⁻¹)	Mode attribution	Intensity
574	Phenyl ring vibration	w
635	Phenyl ring vibration	m
704	C–H bend (o.p.)	m
732	C–H bend (o.p.)	w
761	O–C(O)–O stretch	sh
829	Phenyl ring vibration (o.p.)	sh
836	Phenyl ring vibration	w
888	O–C(O)–O stretch	s
919	C–H bend (i.p.)	w
939	C–H bend (i.p.)	vw
1007	C–H bend (i.p.)	w
1020	C–H bend (i.p.)	w
1080	C–O–C stretch	s
1112	C–O–C stretch	s
1145	C–O–C stretch	s
1180	C–O–C stretch	s
1235	C–O–C stretch	s (broad)
1290	C–O–C stretch	w
1310	C–O–C stretch	w
1372	u	sh
1396	C H ₃ def	sh
1442	C H ₃ symmetric bend	w
1470	C H ₃ asymmetric bend	w
1595	Phenyl ring stretch	sh
1604	Phenyl ring stretch	s
1774	C=O stretch	w
2873	C–H stretching	s
2914	C–H stretching	s
2942	C–H stretching	s
2972	C–H stretching	s
3075	C–H stretching	s

w weak, sstrong, m medium, vw very weak, o.p. out-of-plane, i.p. in plane

parameters, orientation information can not be directly related to raw intensity. However, the ratio of intensities of specific modes are easily used to determine molecular orientation. Similar work was done to determine chain orientation in polyethylene terephthalate,^[19] where the certain modes that are orientation-independent are used for normalization of spectra. Therefore, ratios of intensities of orientation-dependent modes to those of orientation-independent modes is used to quantify orientation.

Determining modes that are orientation-independent and those that are orientation-dependent is not straightforward; absolute Raman intensities can change not only due to orientation, but also due to surface quality. There are disagreements in the literature as to what modes to use for normalization.^[19,27] We used principal component analysis to help differentiate modes that are the least dependent on orientation from those

that are sensitive to orientation eliminating the need for normalization of the spectra. Figure 4(a) shows the score plot of different spectra from different DRs and at angles 0° and 90°. The first principal component (PC1), represented on the horizontal axis, accounts for 80 % of the variance in the intensities of modes and is due to the different DRs. The two spectra at angles 0° and 90° of a single sample mostly have the same projection on PC1. Most importantly, the second principal component (PC2), on the vertical axis, accounts for 14 % of the variance in mode intensities due to the orientation of the samples. All samples measured at 0° are in the upper two quadrants, while those measured at 90° line up in the lower two quadrants. Figure 4(b) shows the loading plot showing the relationship between vibrational modes and PC2. Certain modes seem to show little to no change with orientation such as modes at 640 cm⁻¹ and 709 cm⁻¹, while modes that are most sensitive to orientation are the C–O–C stretch at 1112 cm⁻¹ and 1235 cm⁻¹ and the phenyl ring stretch at 1600 cm⁻¹. In highly oriented samples, the direction of vibration of the C–O–C bond in the stretching mode is approximately parallel to the main chain, and tends to align parallel to the draw direction. Therefore, the intensity of the spectrum in the stretching region 800 cm⁻¹ to 1300 cm⁻¹ is stronger for the parallel polarization direction than for the perpendicular polarization direction. Using the mode at 709 cm⁻¹ as the normalizing mode was determined to be better than the mode at 640 cm⁻¹ due to the higher intensity of the 709 cm⁻¹ and lower signal-to-noise ratio especially when fitting the modes. Therefore, the ratio of intensities of the mode at 1602 cm⁻¹ to that at 709 cm⁻¹ is studied at different DRs.

Figure 5(a) shows a summary of the all drawn samples. Each black point represents Raman measurements from a single sample that was drawn to a specific DR, and every red point is the birefringence (Δn) of that sample. The y-axis on the right is birefringence measurements and on the left is the ratio of intensity of the phenyl ring stretch 1602 cm⁻¹ mode to that of C–H out-of-plane bending at 709 cm⁻¹ at 90° subtracted from the same ratio at 0°:

$$R = \frac{I_{1602}^0}{I_{709}^0} - \frac{I_{1602}^{90}}{I_{709}^{90}} \quad (1)$$

where I is the intensity of the mode (subscript) and superscript represents the angle at which the spectra was measured. To calculate R in Eq. 1, the background was subtracted from all the spectra and then modes were fitted individually with Voigt profiles where the peak heights can be determined for modes at 709 cm⁻¹ and 1602 cm⁻¹. The plot shows strong correlation between the Raman and birefringence measurements for $DR < 3$, the change in behavior of birefringence or Raman intensities with respect to the DR changes dramatically at $DR > 3$ due to grip failure in the solid analyzer. Figure 5(b) shows a plot of the same Raman measurements versus birefringence where a linear relation can be established between the two methods: $\Delta n \approx 21 \times R$. Error bars are the uncertainties/

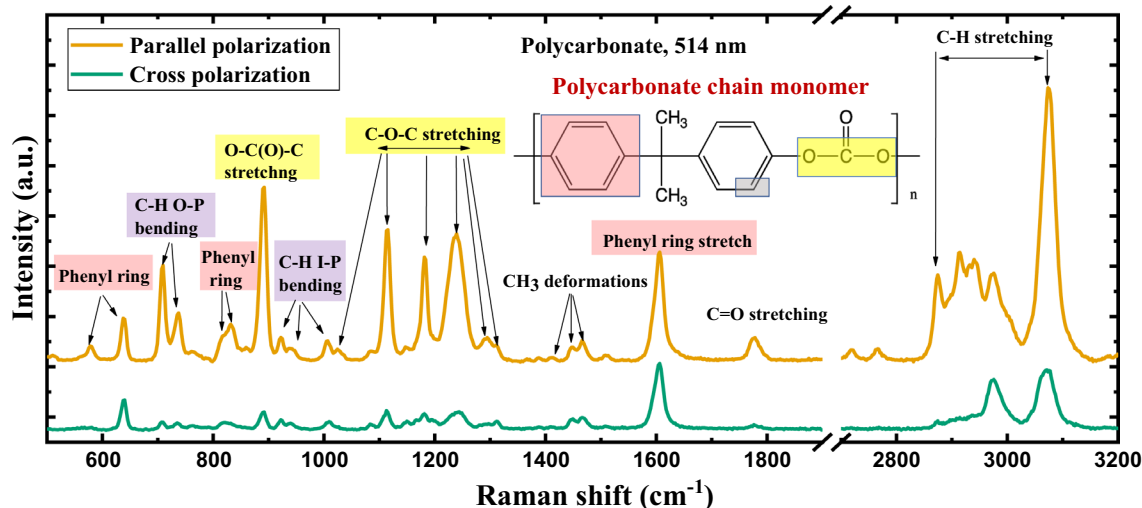


Figure 3. Raman spectra of extruded filaments; vibrational modes of different parts of the monomer are highlighted in color in both the spectrum and the top schematic of the monomer. Cross and parallel polarization are plotted with an offset.

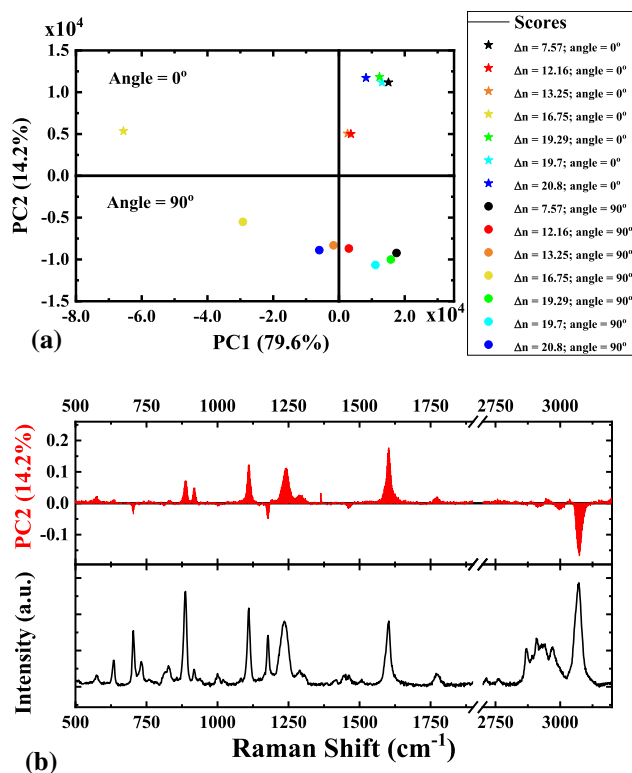


Figure 4. (a) Score plot of Raman measurements collected from filaments at different DRs and at different angles. PC1 is on x-axis accounting for 80 % and PC2 on y-axis accounting for 14 % of the variance. Measurements collected at 0° cluster in the top two quadrants and measurements taken at 90° cluster in the bottom two quadrants. (b) Plot at the bottom is the Raman spectra of PC in the parallel polarization; plot at top is the loading plot of PC2 shows how strongly each mode influences PC2.

standard deviation calculated from repeated Raman measurements of each sample.

A more robust method to relate birefringence to Raman measurements data is using partial least squares (PLS) regression. Without the need to curve fit the peaks, all data from pulled samples can be used as a training set to find birefringence as a function of Raman intensities:

$$\Delta n = \alpha + \sum_{j=freq_i}^{freq_f} \beta_j I_j \quad (2)$$

where β is a scalar multiplier for the intensity at each wave-number to be calculated using PLS regression and α is an offset value. All spectra were initially scaled to the maximum integrated counts of the 640 cm^{-1} mode among all measured spectra and then normalized to peak height of the 640 cm^{-1} mode. Then for each sample, spectrum measured 90° was subtracted from that measured at 0°. Only samples with DR < 3 were used. Figure 6(a) shows a plot of β values vs wave number; it is obvious that some peaks are positively correlated with birefringence and others, such as the C–H modes, are negatively correlated. This method, however, can only provide a birefringence value in the range used in the training set for the PLS regression and performs poorly outside that range. Figure 6(b) shows that percentage difference between the measured birefringence and the calculated birefringence using PLS regression in the training set; all show a less than 5 % difference.

Even though measuring spectra at 0° and 90° is the norm for measuring chain orientation, previous work on PC^[27] observed changes between spectra measured at 0° and 45° where spectra measured at 0° and 90° were non-distinguishable. As a result, measurements were taken for the same samples above but at 0° and 45°. Data show modes at 640 cm^{-1}

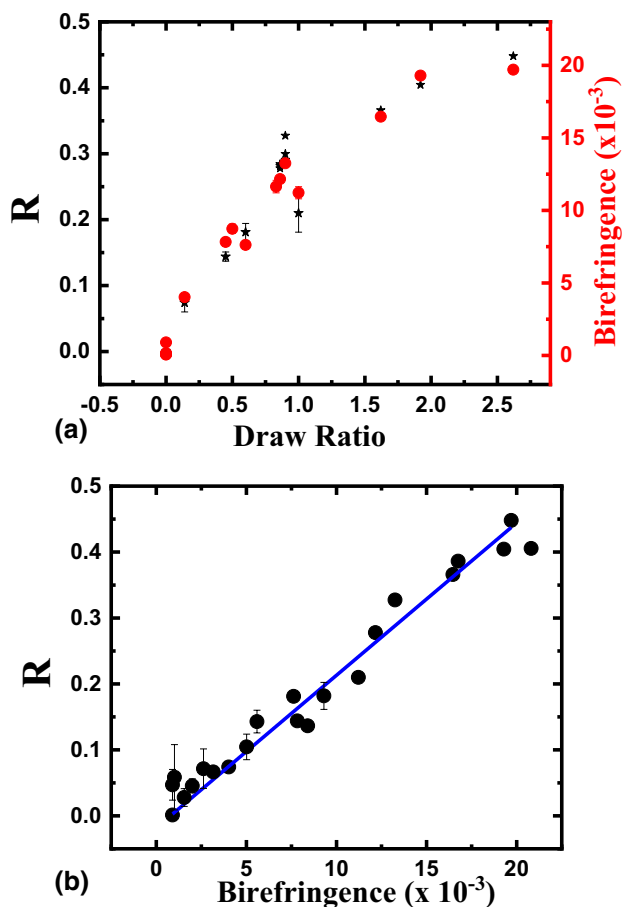


Figure 5. (a) Plots of R calculated in Eq. 1 vs draw ratio in (a) and birefringence in (b) to show relation between Raman scattering data and birefringence measurements. Black: plot of ratio of intensities of Raman modes at 1602 cm^{-1} and 709 cm^{-1} at 90° subtracted from the same ratio at 0° , see Eq. 1, vs DR. Red: birefringence measurements. Both birefringence and ratio of intensities show same behavior with draw ratio. b) Plot of ratio of intensities of Raman modes at 1602 cm^{-1} and 709 cm^{-1} at 90° subtracted from the same ratio at 0° vs birefringence. Blue line is a linear fit. Uncertainty is equal to the standard deviation as determined by repeated measurements.

and 1602 cm^{-1} are orientation-independent, while the rest of the modes are orientation-dependent. That is very different from the situation when comparing spectra collected at angles 0° and 90° , where the 1602 cm^{-1} mode was sensitive to orientation. It is proposed that the change in spectra between angles 0° and 45° is due to birefringence effect on the polarization of scattered radiation. Therefore, depolarized modes such as the ones at 640 cm^{-1} and 1602 cm^{-1} are not affected by rotating the sample while polarized modes such as those at 890 cm^{-1} , 1112 cm^{-1} , and 1235 cm^{-1} are dependent on sample position. In other words, the fact that all polarized modes irrespective of their location on the monomer behave the same (decrease in intensity) suggests that this behavior may be due to birefringence effects. While measuring at parallel polarization either in the parallel or perpendicular

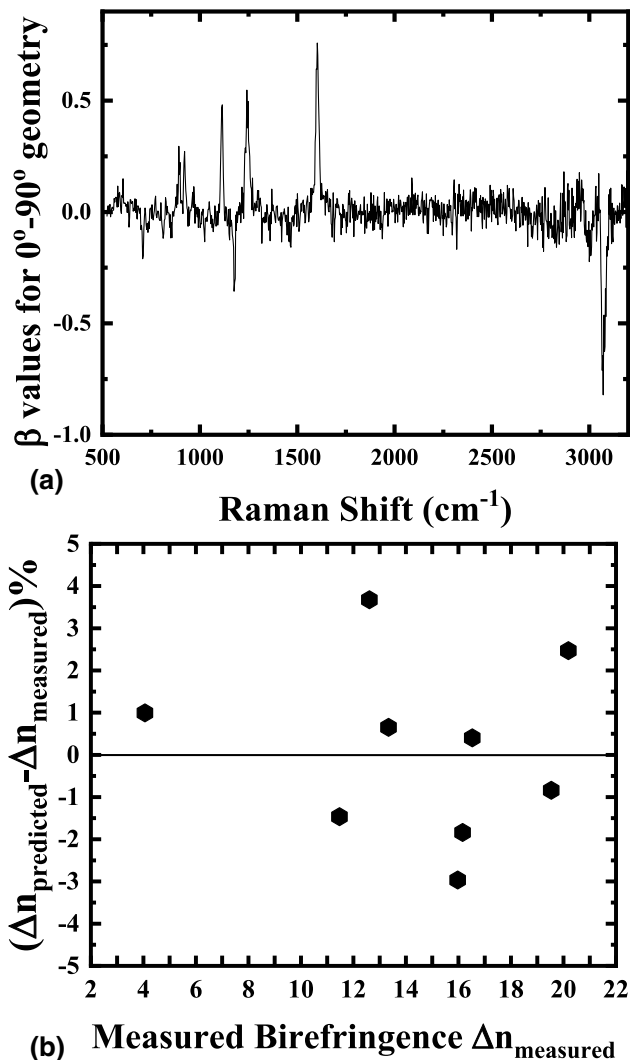


Figure 6. (a) Plot of coefficient, β , calculated from PLS regression of spectra measured at 0° and 90° angles. Modes at 890 cm^{-1} , 1112 cm^{-1} , 1180 cm^{-1} , 1235 cm^{-1} , 1602 cm^{-1} , and 3068 cm^{-1} have the largest coefficients and so determine the birefringence. (b) Plot of percent difference between $\Delta n_{\text{calculated}}$ and $\Delta n_{\text{measured}}$

configuration the polarized light passes through the optical axis or perpendicular to it so experiences in either case one refractive index whether n_1 or n_2 . However, at 45° , the incident polarized light from the laser travels at an oblique angle with respect to the optical axis of the filament. Thus, the two components of the incident light, one component parallel and the other perpendicular to the filament optical axis, experience two different refractive indices which converts the incident and scattered radiation into an elliptically polarized light. Therefore, the analyzer would only let a fraction of the intensity of the elliptical scattered radiation to the detector. This results in that the polarized modes are the most affected and thus decrease in intensity, while depolarized modes do not. It was found that the ratio of intensities of modes

890 cm^{-1} to 640 cm^{-1} provide the most sensitive measure of chain orientation. Figure 8(a) shows that there is almost a linear relation between the birefringence of the samples and the difference in intensity ratios of the formerly mentioned modes at 0° and 45° angles:

$$R' = \frac{I_{890}^0}{I_{640}^0} - \frac{I_{890}^{45}}{I_{640}^{45}} \quad (3)$$

where I is the intensity of the mode (subscript) and superscript represents the angle at which the spectra was measured. The linear relation only applies until a certain DR where the birefringence is around $\approx 10^{-2}$. At larger DR, the Raman values tend to saturate. By applying a rough linear fit to the linear portion of the curve, we get $\Delta n \approx 179 \times R'$ where R' is calculated from Eq. 3.

It is immediately obvious that comparing spectra at 0° and 45° is more sensitive to orientation than using spectra at 0° and 90° angles in samples that were pulled at $DR < 0.7$ or for samples that are expected to have a very small birefringence $< 10^{-2}$. However, for samples that were pulled at $DR > 0.7$ or with high orientation, measuring spectra at 0° and 90° angles is a better predictor of birefringence. Also, PLS regression was used to arrive at an equation, Eq. 2, with a new set of coefficients, β that can be used to predict birefringence given Raman data. Figure 7(a) shows the plot of β vs the frequency, while Fig. 7(b) shows the percentage difference between measured and calculated birefringence values.

Now that we have a method to find birefringence from Raman measurements, we apply the method to calculate the birefringence of 3D printed samples in the region of the laser spot (approximately 1 μm) and compare to the birefringence measured from transmission mode optical imaging. Four samples were printed at temperatures 220 °C, 240 °C, 260 °C, and 280 °C. It is expected that filaments printed at 220 °C experience less relaxation and lose less of the gained orientation from the unavoidable shear before solidification, and as a result will have the highest orientation. The minimum weld strength is thus expected in samples prepared at the lowest extruder temperature and at the slowest extruder speed.^[5] Raman measurements on samples printed at 220 °C were measured at 0°, 45°, and 90° degrees. Minimal orientation was detected in these samples especially when comparing spectra taken at 0° and 90°; see Fig. 9a(). Figure 9(b) shows a plot of Raman spectra taken at 0° and 45° angles, and the difference between the two spectra is shown in black. Using the linear relation, or PLS regression and comparing the ratio of intensities of modes 890 cm^{-1} to 640 cm^{-1} to those of drawn samples, we find that the local birefringence in the region of the Raman spot is in the range 1×10^{-3} to 2×10^{-3} . This birefringence corresponds to that measured in samples cold drawn at a DR in the range 0.04 and 0.1. More interesting is that the measured birefringence of all 3D printed samples from optical imaging was in the range from 6×10^{-5} to 14×10^{-5} , an order of magnitude less than the Raman-derived local birefringence. Our

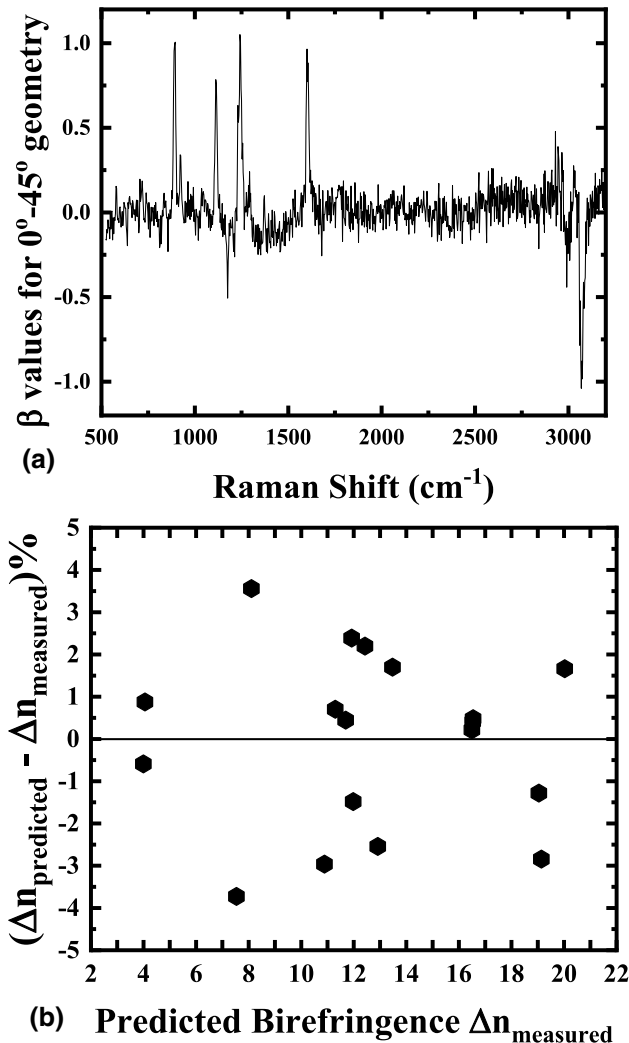


Figure 7. (a) Plot of coefficient, β , calculated from PLS regression of spectra measured at 0° and 45° angles. Modes at 709 cm^{-1} , 890 cm^{-1} , 1112 cm^{-1} , 1180 cm^{-1} , 1235 cm^{-1} , 1602 cm^{-1} , and 3068 cm^{-1} have the largest coefficients and so determine the birefringence. (b) Plot of percent difference between $\Delta n_{\text{calculated}}$ and $\Delta n_{\text{measured}}$.

measurements confirm that transmission-based birefringence measurements, see Fig. 10, are a poor measure of chain orientation in weakly oriented 3D printed samples. Because the shear is most pronounced on the surface of the samples with almost no orientation in the core, transmission methods tend to underestimate chain orientation and thus a surface method such as Raman spectroscopy is more sensitive and can be used to evaluate birefringence and the orientation function. However, Raman spectra of samples printed at 240 °C, 260 °C, and 280 °C were indistinguishable at angles 0°, 45°, and 90° and thus, implying that orientation is minimal and below the threshold of Raman sensitivity. By comparing to birefringence values of pulled samples, we can conclude that the birefringence of these samples is $< 0.8 \times 10^{-3}$. With intrinsic birefringence of

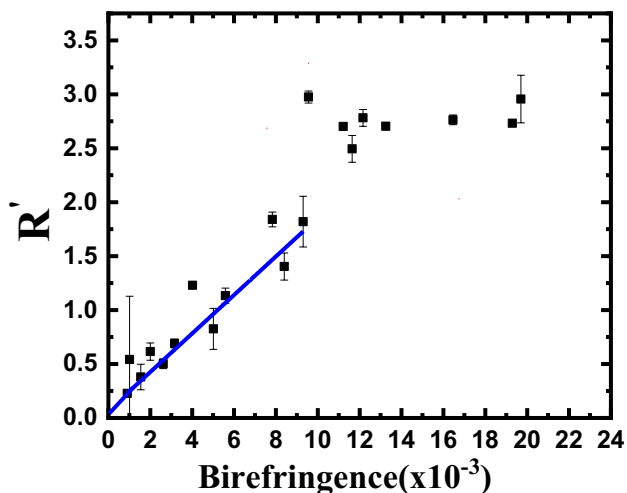


Figure 8. Plot of ratio of intensities of different Raman modes at 890 cm^{-1} cm to those at 640 cm^{-1} cm at 45° subtracted from those at 0° for pulled extrudate vs birefringence. There is a plateau that is reached for birefringence $\Delta n > 10^{-2}$. Uncertainty is equal to the standard deviation as determined by repeated Raman measurements.

PC $\Delta n_{\text{intrinsic}} \approx 0.2$,^[33,34] we can estimate the maximum value for Herman's orientation function (f) as:

$$f = \frac{\Delta n}{\Delta n_{\text{intrinsic}}} = 4 \times 10^{-3} \quad (4)$$

Such low monomer or segmental orientation can be explained by comparing reptation times and relaxation time. After extrusion, the printed layer cools down; during that time the chains relax leading to less deformation and orientation via reptation, while inter-diffusing with the previously-printed layer. Therefore, the cooling rate hinders the total relaxation of the deformation induced by shear flow leading to less entanglement and weaker weld-line interface.^[35] At 260°C $\tau_e \approx 0.1\text{ ms}$ and $\tau_d \approx 3\text{ ms}$ based on a fit of the linear rheology using the Likhtman-McLeish^[36] model as implemented in Reptate,^[37] see Fig. S1. The isothermal equivalent relaxation time for the range of temperatures studied is $\approx 10\text{ ms}$.^[38] From these timescales we can expect relaxation of monomers or statistical segments and partial relaxation of the tube or end-to-end vector. Thus, theoretical models^[7,39] and thermal measurements^[2,38] could explain the low orientation in 3D printed PC samples. That raises the question if such low orientation is still responsible for the weak mechanical properties in the weld area or whether other mechanisms are more crucial.

Conclusion

In conclusion, we detailed a method to relate birefringence and Raman measurements that can be employed in any polymer. Such method is best used in situations where the orientation

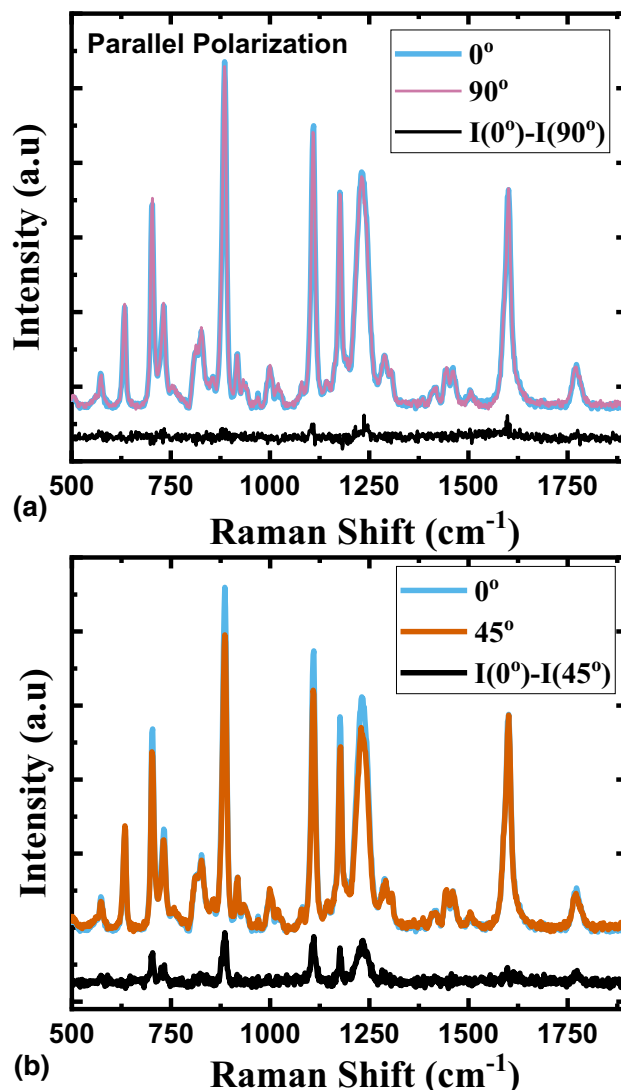


Figure 9. Spectra of filaments after extrusion at 220°C . (a) Comparison between Raman spectrum (parallel polarization) of extruded filaments at 0° (blue) and 90° (pink/violet). The difference between the two spectra is shown in black (offset). (b) Comparison between Raman spectrum of extrudate (extruded at 220°C) at 0° (blue) and 45° (brown). The difference between the two spectra is shown in black.

is highest on surface and thus Raman, a surface method, is preferred. First PCA can be used to easily determine which modes are orientation-independent to be used for normalization and which modes are orientation sensitive. PLS regression was used to relate Raman intensities to birefringence. For samples with high orientation, a geometry is preferred where Raman measurements are measured at 0° and 90° angles, whereas low orientation sample, measurements at 0° and 45° angles are more sensitive to molecular orientation. In either case, Raman is not sensitive to samples with $\text{DR} < 0.04$ or birefringence less than 1×10^{-3} . For 3D printed PC samples at 220°C , birefringence is calculated to be around 1×10^{-3} similar to samples that were pulled at DR in the range from 0.04 to 0.1. Samples printed at

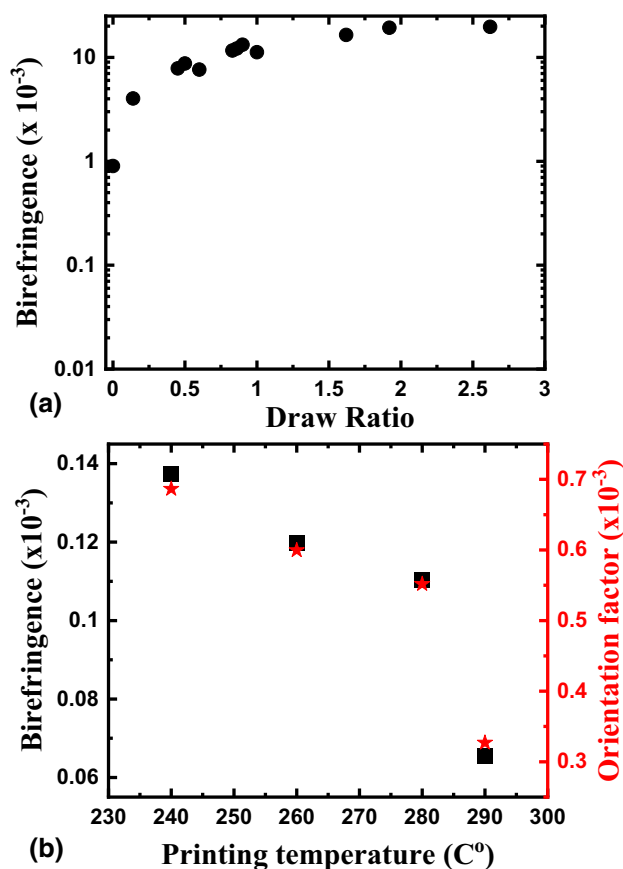


Figure 10. (a) Comparison between birefringence measured on pulled samples with different DRs in black. Birefringence of printed sample is one order of magnitude smaller than those of pulled samples even at DR as small as 0.14. (b) Plot of measured birefringence of extrudate from the 3D printer versus printing temperature. Calculated orientation function from the birefringence is plotted on the right axis in orange.

higher temperature show much less orientation that is below Raman sensitivity.

Acknowledgments

The authors would like to thank Marco A. G. Cunha and the late Mark O. Robbins for their invaluable discussions on relaxation processes during flow. This work was supported by the National Institute of Standards and Technology (NIST) Scientific and Technical Research and Services (STRS) and by the National Science Foundation (NSF) under Grant Number NSF DMREF-90069795.

Data availability

The data that support the findings of this study are available from the corresponding author upon reasonable request.

Declarations

Conflict of interest

On behalf of all authors, the corresponding author states that there is no conflict of interest.

Supplementary Information

The online version contains supplementary material available at <https://doi.org/10.1557/s43579-021-00025-z>.

References

1. J.P. Davim, *Machining: Fundamentals and Recent Advances*, Springer, London, ISBN 978-1-84800-212-8, (2008)
2. J.E. Seppala, S.H. Han, K.E. Hillgartner, C.S. Davis, K.B. Migler, Weld formation during material extrusion additive manufacturing. *Soft Matter* **13**, 6761–6769 (2017)
3. T.J. Coogan, D.O. Kazmer, Healing simulation for bond strength prediction of FDM. *Rapid Prototyp J* **23**, 11 (2017)
4. C.S. Davis, K.E. Hillgartner, S.H. Han, J.E. Seppala, Mechanical strength of welding zones produced by polymer extrusion additive manufacturing. *Addit Manuf* **16**, 162–166 (2017)
5. L. Fang, Y. Yan, O. Agarwal, J.E. Seppala, K.J. Hemker, S.H. Kang, Processing-structure-property relationships of bisphenol-A-polycarbonate samples prepared by Fused Filament Fabrication. *Addit Manuf* **35**, 101285 (2020)
6. K.R. Hart, E.D. Wetzel, Fracture behavior of additively manufactured acrylonitrile butadiene styrene (ABS) materials. *Eng Fract Mech* **177**, 1–13 (2017)
7. C. McIlroy, P. Olmsted, Disentanglement effects on welding behaviour of polymer melts during the fused-filament-fabrication method for additive manufacturing. *Polymer* **123**, 376–391 (2017a)
8. A. Costanzo, R. Spotorno, M.V. Candal, M. J. Fernández, A. J. Müller, G. R. S. D. Cavallo, C. McIlroy, Residual alignment and its effect on weld strength in material-extrusion 3D-printing of polylactic acid. *Addit Manuf* **36**, 101415 (2020)
9. I.M. Ward, *Structure and Properties of Oriented Polymers* (Springer, Berlin, 1975)
10. K. Kojio, T. Kajiwara, S. Yamamoto, A. Fujimoto, K. Fukada, C. Nagano, S. Masuda, C.-H. Cheng, S. Nozaki, K. Kamitani, A. Takahara, Direct visualization of the molecular orientation and microstructure of glassy transparent polymers after the scratch test based on optical microscopy and X-ray scattering. *Polymer* **181**, 121773 (2019)
11. H.J. Biangardi, Determination of the orientation distribution function of amorphous polymers by wide angle X-ray scattering measurements. *Makromol Chem* **183**, 1785–1802 (1982)
12. G. Voyiatzis, G. Petekidis, D. Vlassopoulos, E.I. Kamitsos, A. Bruggeman, Molecular orientation in polyester films using polarized laser Raman and Fourier transform infrared spectroscopies and X-ray diffraction. *Macromolecules* **29**(6), 2244–2252 (1996)
13. R. Wimbercer-Fried, J.G.D. Bruin, Birefringence in polycarbonate: molecular orientation induced by cooling stresses. I. Free quenching. *J Polym Sci* **31**, 1041–1049 (1993)
14. C.W. Lantman, J.F. Tassin, L. Monnerie, L.J. Fetters, E. Helfand, D.S. Pearson, Fourier transform infrared dichroism study of orientation relaxation using isotopically labeled polystyrene stars. *Macromolecules* **22**, 1184–1188 (1989)
15. C.Y. Lang, S. Krimm, Infrared spectra of high polymers. *J Mol Spectrosc* **3**, 554–574 (1959)
16. S. Krimm, Infrared spectra of high polymers, in *Advances in Polymer Science*, vol. 2, ed. by T. Krimm (Springer, Berlin, 1960), pp. 51–172
17. J. Guèvremont, A. Aiji, K.C. Cole, M.M. Dumoulin, Orientation and conformation in poly(ethylene terephthalate) with low draw ratios as characterized by specular reflection infra-red spectroscopy. *Polymer* **36**(17), 3385–3392 (1995)

18. N. Everall, P. Tayler, J.M. Chalmers, D. MacKerron, R. Ferwerda, J.H. van der Maas, Study of density and orientation in poly(ethylene terephthalate) using Fourier transform Raman spectroscopy and multivariate data analysis. *Polymer* **35**(15), 3184–3192 (1994)
19. S. Natarajan, S. Michielsen, Determination of density and birefringence of poly(ethylene terephthalate) fibers using Raman microscopy. *J Appl Polym Sci* **73**, 943–952 (1999)
20. M. Pigeon, R.E. Prudhomme, M. Pézolet, Characterization of molecular orientation in polyethylene by Raman spectroscopy. *Macromolecules* **24**, 5687–5694 (1991)
21. D. Purvis, D.I. Bower, A study of molecular orientation in poly(methyl methacrylate) by means of laser-Raman spectroscopy. *Polymer* **15**, 645–654 (1974)
22. D.I. Bower, Investigation of molecular orientation distributions by polarized Raman scattering and polarized fluorescence. *J Polym Sci* **10**, 2135–2153 (1972)
23. S. Yang, S. Michielsen, Orientation distribution functions obtained via polarized Raman spectroscopy of poly(ethylene terephthalate) fibers. *Macromolecules* **36**(17), 6484–6492 (2003)
24. A. Soto, G. A. Voyiatzis, Molecular orientation of poly(ethylene naphthalate) \ poly(ethylene terephthalate) copolymers utilizing polarized Raman spectra. *Macromolecules* **2002**, 35, 2095–2104 *35* (6) (2002) 2095–2104
25. J. Pruvius, D.I. Bower, Molecular orientation in poly(ethylene terephthalate) by means of laser-Raman spectroscopy. *J Polym Sci* **14**, 1461–1484 (1976)
26. M.J. Citra, D.B. Chase, R.M. Ikeda, K.H. Gardner, Molecular orientation of high-density polyethylene fibers characterized by polarized Raman spectroscopy. *Macromolecules* **28**(11), 4007–4012 (1995)
27. M. Takeshima, N. Funakoshi, Molecular orientation distribution in injection-molded polycarbonate discs. *J Appl Polym Sci* **32**, 3457–3468 (1986)
28. M.A.G. Cunha, M.O. Robbins, Effect of flow-induced molecular alignment on welding and strength of polymer interfaces. *Macromolecules* **53**(19), 8417–8427 (2020)
29. J. Bent, L.R. Hutchings, R.W. Richards, T. Gough, R. Spares, P.D. Coates, I. Grillo, O.G. Harlen, D.J. Read, R.S. Graham, A.E. Likhtman, D.J. Groves, T.M. Nicholson, T.C.B. McLeish, Neutron-mapping polymer flow: scattering, flow visualization, and molecular theory. *Science* **301**(5640), 1691–1695 (2003)
30. R.S. Graham, J. Bent, L.R. Hutchings, R.W. Richards, D.J. Groves, J. Embery, T.M. Nicholson, T.C.B. McLeish, A.E. Likhtman, O.G. Harlen, D.J. Read, T. Gough, R. Spares, P.D. Coates, I. Grillo, Measuring and predicting the dynamics of linear monodisperse entangled polymers in rapid flow through an abrupt contraction. A small angle neutron scattering study. *Macromolecules* **39**(7), 2700–2709 (2006)
31. T.C. Damen, S.P.S. Porto, B. Tell, Raman effect in zinc oxide. *Phys Rev* **142**, 570–574 (1966)
32. V. Resta, G. Quarta, M. Lomascolo, L. Maruccio, L. Calcagnile, Raman and photoluminescence spectroscopy of polycarbonate matrices irradiated with different energy $^{28}\text{Si}^+$ ions. *Vacuum* **116**, 82–89 (2015)
33. M. Pietralla, T. Pieper, The problem of intrinsic birefringence and chain conformation in polycarbonate from bisphenol-A. *Colloid Polym Sci* **268**(9), 797–805 (1990)
34. M.S. Wu, Intrinsic birefringence of amorphous poly(bisphenol-A carbonate). *J Appl Polym Sci* **32**, 3263–3275 (1986)
35. T.C. O'Connor, A. Hopkins, M.O. Robbins, Stress relaxation in highly oriented melts of entangled polymers. *Macromolecules* **52**(8540–8550), 22 (2019)
36. A.E. Likhtman, T.C.B. McLeish, Quantitative theory for linear dynamics of linear entangled polymers. *Macromolecules* **35**(16), 6332–6343 (2002)
37. V.A.H. Boudara, D.J. Read, J. Ramirez, Reptate rheology software: toolkit for the analysis of theories and experiments. *J Rheol* **64**(3), 709–722 (2020)
38. J.E. Seppala, K.D. Migler, Infrared thermography of welding zones produced by polymer extrusion additive manufacturing. *Addit Manuf* **12**(Part A), 71–76 (2016)
39. C. McLroy, P.D. Olmsted, Deformation of an amorphous polymer during the fused-filament-fabrication method for additive manufacturing. *J Rheol* **61**, 379–397 (2017b)